



# Kahramanmaraş Sutcu Imam University

## Journal of Engineering Sciences



Geliş Tarihi : 14.12.2025  
Kabul Tarihi : 21.02.2026

Received Date : 14.12.2025  
Accepted Date : 21.02.2026

### MULTI-VARIABLE OPTIMIZATION OF PHYSICAL AND MECHANICAL PROPERTIES OF HYBRID ALKALI-ACTIVATED BLAST FURNACE SLAG MORTARS

### ALKALİ İLE AKTİVE EDİLMİŞ YÜKSEK FIRIN CÜRUFULU HİBRİT ÇİMENTO HARÇLARININ FİZİKSEL VE MEKANİK ÖZELLİKLERİNİN ÇOKLU OPTİMİZASYONU

*Yunus Emre AVŞAR*<sup>1\*</sup> (ORCID: 0000-0001-5197-0267)

*Mehmet Timur CİHAN*<sup>1</sup> (ORCID: 0000-0001-5555-5589)

*İbrahim Fedâ ARAL*<sup>1</sup> (ORCID: 0000-0002-5526-472X)

<sup>1</sup> Tekirdağ Namık Kemal Üniversitesi, İnşaat Mühendisliği Bölümü, Tekirdağ, Türkiye

\*Sorumlu Yazar / Corresponding Author: Yunus Emre AVŞAR, yeavsar@nku.edu.tr

#### ABSTRACT

Multi-variable optimization of physical and mechanical properties of hybrid alkali-activated blast furnace slag (BFS) mortars was investigated. Portland cement (PC), BFS, sodium metasilicate ( $\text{Na}_2\text{SiO}_3$ ), standard sand, distilled water, and superplasticizer were used in the production of hybrid alkali-activated cement (HAAC) mortar specimens. An Optimal (Combined) Custom Design was used in the study to produce HAAC with optimum mechanical and physical properties, focusing on selected effect variables. The run points that provided the optimum mechanical, physical, and mechanical/physical properties were determined by using the desirability function. The results show that the addition of PC to the mixture does not improve mechanical properties but it does improve physical properties. The desirability values are obtained as 1, 1, and 0.913, for the mechanical (100% PC), physical (60% PC), and mechanical/physical (60% PC) properties in HAACs, respectively. Therefore, for the usability of HAACs, it is crucial to determine the optimum conditions based on environmental factors and design accordingly.

**Keywords:** Hybrid alkali-activated cement (HAAC), mechanical and physical properties, analysis of variance (ANOVA), optimization, sustainability

#### ÖZET

Bu çalışmada alkali ile aktive edilmiş yüksek fırın cürufulu (YFC) hibrit harçların fiziksel ve mekanik özelliklerinin çoklu optimizasyonu araştırılmıştır. Alkali ile aktive edilmiş hibrit çimento harç (HAAC) numunelerinin üretiminde Portland çimentosu (PÇ), YFC, sodyum metasilikat ( $\text{Na}_2\text{SiO}_3$ ), standart kum, distile su ve süperakışkanlaştırıcı kullanılmıştır. Çalışmada, seçilen etki değişkenlerine odaklanarak optimum mekanik ve fiziksel özelliklere sahip HAAC üretmek için Optimal (Kombine) Tasarım kullanılmıştır. Optimum mekanik, fiziksel ve mekanik/fiziksel özellikleri sağlayan deneme noktaları, arzu edilebilirlik fonksiyonu kullanılarak belirlenmiştir. Sonuçlar, PÇ ilavesinin mekanik özellikleri iyileştirmediğini fakat fiziksel özellikleri iyileştirdiğini göstermektedir. HAAC'larda mekanik (100% PÇ), fiziksel (60% PÇ) ve mekanik/fiziksel (60% PÇ) özellikler için arzu edilebilirlik değerleri sırasıyla 1, 1 ve 0.913 olarak elde edilmiştir. Bu nedenle, HAAC'ların kullanılabilirliği için, çevresel faktörlere dayalı olarak optimum koşulları belirlemek ve buna göre tasarım yapmak çok önemlidir.

**Anahtar Kelimeler:** Alkali ile aktive edilmiş hibrit çimento (HAAC), mekanik ve fiziksel özellikler, Varyans analizi (ANOVA), optimizasyon, sürdürülebilirlik

## INTRODUCTION

The substantial CO<sub>2</sub> emissions for the Portland cement (PC) production and the extensive use of energy and natural resources have prompted the scientific community to seek alternative materials with similar physical and mechanical properties to PC yet produced more sustainably. These materials are environmentally friendliness (García-Lodeiro et al., 2012; Law et al., 2012; Schneider et al., 2011; Scrivener et al., 2011; Yang et al., 2008). Presently, an increasingly innovative choice is known as hybrid alkali-activated cement (HAAC). These cementitious substances use significant proportions of industrial by-products, like blast furnace slag (BFS) or fly ash (FA) (Angulo-Ramírez et al., 2017).

The workability, slump, and setting time are decreased when the PC replacement ratio to the alkali-activated BFS increases at the HAAC (Ameri et al., 2020; Francis Yakobu et al., 2015; Khan et al., 2014; Shoaie et al., 2020). It was determined that 20% and 30% PC substitution reduced workability by 84% and 92%, respectively (Amer et al., 2021). In another study, a decrease in the slump value of HAAC concrete was observed with an increase in the PC ratio (0% PC: 122 mm, 60% PC: 30 mm) (Askarian et al., 2018). In addition, PC addition decreased workability due to increased angular particles (Jindal, 2019; Provis et al., 2010). The time required for HAACs to solidify is reduced since alkali activators in HAACs accelerate PC hydration (Xue et al., 2021). When the PC ratio was increased from 0% to 50%, the initial setting time was shortened from 350 to 140 min. It could be explained by the smoother surface texture of BFS particles than cement particles, which causes a delay in the chemical reaction and setting time (Francis Yakobu et al., 2015). Higher PC substitution leads to rapid setting due to the flash chemical reaction between PC and alkali activators (Askarian et al., 2018). For example, Suwan & Fan (2014) determined the setting time of HAAC paste as 22 and 11 min for 50% and 70% PC replacement, respectively.

It was reported that the HAAC sample (80% BFS and 20% PC) achieved compressive strength ( $f_c$ ) 10.8 times higher than the control sample (100% PC) (Angulo-Ramírez et al., 2017).  $f_c$  of HAAC is influenced significantly by the PC content in the mixture (Fang et al., 2018; Nath & Sarker 2014; Patel & Shah 2018; Saha & Rajasekaran 2017). When the PC ratio increased from 10% to 30%, the  $f_c$  decreased from 56.4 to 21.9 MPa (Fang et al., 2018). In another study, 20% and 30% PC substitution reduced the compressive strength by 20% and 45%, respectively (Amer et al., 2021). This situation may be due to the activator's effect on hydration. There is a notable accumulation of Na-substituted C-S-H (N-C-S-H) and Ca(OH)<sub>2</sub> because of this effect. These formations exhibit lower density than the hydration product and consequently possess reduced strength (Bilim & Atiş 2012). Furthermore, the increase in the PC ratio leads to a notable rise in micro-crack formation, resulting in diminished  $f_c$  and a decrease in the uniformity of the hydration products (Amer et al., 2021).

As to durability, decreasing the PC ratio could increase the sulfate and chloride resistance and also reduce the alkali-silica reaction. Impermeable microstructures are formed when more BFS is added (Escalante et al., 2001). The high amount of BFS in the HAAC decreases the concrete's alkalinity, and the low alkalinity significantly reduces the alkali-silica reaction (Topçu, 2013).

Some research was carried out to investigate the optimum constituent materials of HAAC (Fang et al., 2018). It was reported that the mixtures with relatively high BFS content (at least 20%) could obtain a  $f_c$  of 35 MPa. The mixes with BFS replacement of 20% to 30% and an activator/binder ratio of 0.35 to 0.4 can be suggested as optimum mixes (Fang et al., 2018). In another study, the highest CS (78.42 MPa) was achieved at 0.40 activator/BFS ratio (Aliabdo et al., 2019). Amer et al. (2020) determined that the most remarkable variable affecting the 28-day and 7-day CS was the BFS: PC ratio 56.19 and 43.91% attendance percentages, respectively. Avşar and Cihan (2023) determined that the optimum value of Na<sub>2</sub>SiO<sub>3</sub> solution/NaOH solution ratio, total solution/binder ratio, NaOH molarity, Na<sub>2</sub>SiO<sub>3</sub> solution water/Na<sub>2</sub>SiO<sub>3</sub> solution ratio, ultrasonic pulse velocity, flexural strength, and compressive strength are 1.88, 0.4, 11.5, 0.6, 4.18, 6.6, and 45.3, respectively.

The current standards for producing HAAC are lacking, primarily because the HAAC reaction mechanism is complex. Existing standards mainly concentrate on traditional cementitious materials and their characteristics, leaving the optimal mixture design for HAAC largely unexplored (Shi et al., 2022). It is crucial to evaluate the effect of various factors to understand the mechanical and physical behaviour of HAAC. An Optimal (Combined) Custom Design was used in the study to produce HAAC with optimum mechanical and physical properties, focusing on selected effect variables.

Strength-to-durability optimization of concrete is a complex task, requiring consideration of various factors to achieve desired performance outcomes. Therefore, experimental designs like the Rotatable Central Composite Design (Avşar & Cihan, 2023) and the Taguchi method (Amer et al., 2021) have been used to optimize the controllable design parameters. While the Taguchi method is robust for optimizing concrete performance, it is limited in addressing multiple quality responses, as it focuses on a single criterion. This constraint has led to the prominence of multi-objective optimization methods, which excel in handling multi-response problems (Chokkalingam et al., 2022). The desirability method, a mathematical venture to determine the optimal value or property (StatEase, 2021a), was applied to optimize multi-response problems in the study.

To understand HAACs, finding the optimum values of the variables that affect their properties is crucial. This research aimed to determine the optimum values of variables, focusing on the mechanical and physical properties of HAAC mortars through a multi-response optimization. The objectives of this study are determining the effect levels of the variables on the response variables, reducing PC usage, and promoting environmental sustainability by incorporating industrial waste materials like BFS.

## MATERIALS AND METHODS

### Materials

CEM I 42.5 R Portland cement (PC), CEN standard sand (SS), distilled water, blast furnace slag (BFS), and sodium metasilicate ( $\text{Na}_2\text{SiO}_3$ ) were used in the production of hybrid alkali-activated cementitious (HAAC) mortar specimens according to TS EN 196-1 (2016). The workability of the mortars was kept constant in the range of 10.1-20.4 cm (flow table value) by using a modified polycarboxylate polymer-based liquid high-performance superplasticizer chemical additive (0.1-0.5% by weight of binder). The chemical composition and physical properties of PC and BFS are given in Table 1.

**Table 1.** Chemical Compositions and Physical Properties of PC and BFS

Composition (%)	PC	GBFS
SiO <sub>2</sub>	19.031	40.08
CaO	64.348	31.19
MgO	0.904	7.90
Al <sub>2</sub> O <sub>3</sub>	4.806	13.69
Fe <sub>2</sub> O <sub>3</sub>	2.976	0.90
Cl <sup>-</sup>	0.006	-
SO <sub>3</sub>	3.215	0.26
Na <sub>2</sub> O	-	0.84
K <sub>2</sub> O	-	0.80
Na <sub>2</sub> O + 0,658 K <sub>2</sub> O	1.02	-
Loss of ignition	3.747	4.34
<b>Physical properties</b>		
Specific gravity, g/cm <sup>3</sup>	3.08	2.89
Blaine specific surface, cm <sup>2</sup> /g	3500.00	4452.00

The grain shape properties of the PC and GBFS used in the study were determined using SEM images (grain shape; Figure 1, and surface texture; Figure 2). Figure 1 and Figure 2 show that the PC and GBFS grain shapes are angular and irregular. Moreover, the surface texture of the PC and GBFS grains is smooth.

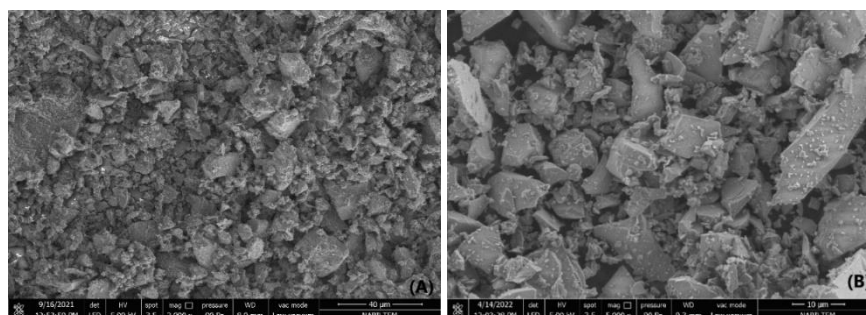


**Figure 1.** Shape Properties/2000x SEM Image of PC (A) and Shape Properties/5000x SEM Image of GBFS (B)

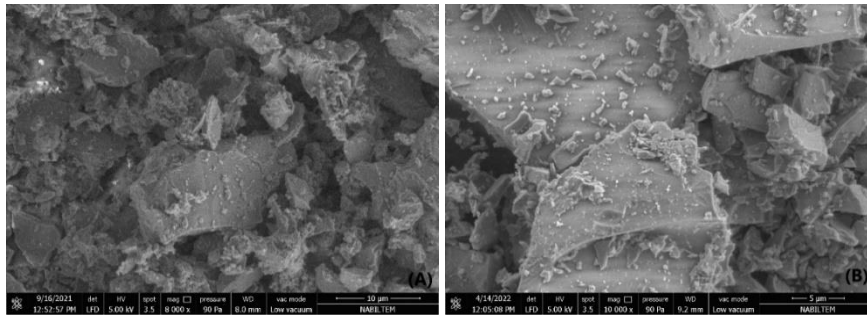


**Figure 2.** Surface Texture Properties/8000x SEM Image of PC (A) and Surface Texture Properties/10000x SEM Image of GBFS (B)

### Methods

The multi-variable optimization of physical, and mechanical properties of the mortars (HAAC) produced using the PC and alkali-activated GBFS were examined in the study. For this purpose, combined and I-optimal were chosen as the study and design types, respectively. PC and GBFS as mixture components, and solution/GBFS, solution water/solution, specimen age, and water/binder as effect (process) variables, unit weight (UW), water absorption (WA), flexural strength ( $f_f$ ), and compressive strength ( $f_c$ ) as response variables were selected. The I-optimal criterion can be applied to create designs for constrained mixture problems. This criterion emphasizes achieving accurate average predictions within the design region and can be implemented by utilizing candidate points or selecting from all possible points within the design region. The design summary of the mixture components and process variables is given in Table 2. The total quantity of binder is 1350 g, and sand/binder ratio is 2.

**Table 2.** Design Summary of Mixture Components and Process Variables

Name	Units	Type	Minimum	Maximum	Coded low	Coded high	
<b>Mixture components</b>							
A	GBFS	%	Mixture	60	100	+0 ↔ 60	+1 ↔ 100
B	PC	%	Mixture	0	40	+0 ↔ 0	+1 ↔ 40
				Total =	100.00	<b>L_Pseudo Coding</b>	
<b>Process factors</b>							
C	Solution/GBFS	%	Numeric	30.00	50.00	-1 ↔ 30.00	+1 ↔ 50.00
D	Solution Water/Solution	%	Numeric	45.00	65.00	-1 ↔ 45.00	+1 ↔ 65.00
E	Specimen age	Day	Numeric	3.00	90.00	-1 ↔ 3.00	+1 ↔ 90.00
F	Water/Binder	%	Numeric	35.00	45.00	-1 ↔ 35.00	+1 ↔ 45.00

Mortar production was carried out as follows: preparation of sodium metasilicate solution, the addition of GBFS to the solution and mixing, addition of SS to the solution + GBFS mixture and mixing, addition of additional water and mixing, addition of superplasticizer and mixing.

The effect levels of the main and interaction terms of the effect variables on the response variables were determined by analysis of variance (ANOVA). For statistical analysis, 55 run points were obtained for statistical analysis, and a total of 330 specimens (square prism, 40×40×160 mm) were produced, 6 for each run point. The experimental results for the run points were calculated by the average of the 4 (for  $f_f$  and  $f_c$ ) and 2 (for UW and WA) specimen values. Experimental design, ANOVA, and response surfaces were performed with the Design Expert Version 13 trial program (StatEase, 2021b). The workability of the mortars was measured with the flow table test according to the TS EN 1015-3 (2000). Unit weight and water absorption of mortar specimens were calculated by Equation 1 and Equation 2, respectively. The flexural and compressive strengths were determined according to the TS EN 196-1 (2016).

$$UW = \frac{ODW}{(SSDW - UWW)/d_w} \quad (1)$$

$$WA = \frac{(SSDW - ODW)}{ODW} \times 100 \quad (2)$$

UW; Unit Weight ( $g/cm^3$ ), WA; Water Absorption (%), SSDW; Saturated Surface Dry Weight (g), UWW; Under Water Weight (g), ODW; Oven Dry Weight (g),  $d_w$ ; density of water ( $g/cm^3$ ).

In cases where the number of design variables ( $> 3$ ) is high, it is necessary to employ a practical general optimization method (Myers et al., 2009). Therefore, in this study, the simultaneous optimization technique (Derringer & Suich, 2018) was used to optimize response variables depending on the selected range of design variables. The simultaneous optimization technique involves the use of desirability functions. The general approach is to transform each response  $y_i$  into a separate desirability function varying in the  $0 \leq d_i \leq 1$ . Here, if the response  $y_i$  is at the target or objective value, then  $d_i = 1$ , and if the response is outside the acceptable region, then  $d_i = 0$ . Moreover, design variables with  $m$  responses are selected to maximize the total desirability,  $D = (d_1 d_2 \dots d_m)^{1/m}$  (Myers et al., 2009).

## RESULTS AND DISCUSSION

In the experimental design, 55 run points were obtained for statistical analysis. The design summary of response variables is given in Table 3. Statistical analysis often involves applying a transformation to response results to stabilize the variance of the response. Transformation not only helps bring the distribution of the response variable closer to a normal distribution but also improves the fitting of the model. The Box-Cox procedure utilizing the principles of the maximum likelihood method is commonly used to determine whether a transformation is necessary for the response variable (Box & Cox 1964). After conducting the Box-Cox analysis, it was concluded that applying the square root transformation to the  $f_r$  and  $f_c$  resulted in an improved model fit (Table 3). However, it was determined that no transformation was necessary for the other response variable results. The run points and test results of response variables are given in Table 4.

**Table 3.** Design Summary of Response Variables

Response Name	Units	Obs*	Analysis	Min	Max	Mean	SD**	Ratio	Transform	Model
R1	WA %	55	Polynomial	6.10984	11.2292	8.76	1.06	1.84	None	Reduced Quadratic x Quadratic Reduced
R2	UW g/cm <sup>3</sup>	55	Polynomial	1.981	2.11275	2.04	0.0277	1.07	None	Quadratic x Quadratic Reduced
R3	$f_r$ MPa	55	Polynomial	0	9.8	5.50	2.45	N/A	Square Root	Quadratic x Quadratic Reduced
R4	$f_c$ MPa	55	Polynomial	0.225	62.0125	26.34	16.39	275.61	Square Root	Quadratic x Quadratic

\*Obs: Observations, \*\*SD: Standard deviation

**Table 4.** Run Points and Test Results of Response Variables

Run points	Space Point Type	Components		Process Factors				Responses			
		A %	B %	C %	D %	E Day	F %	R1 %	R2 g/cm <sup>3</sup>	R3 MPa	R4 MPa
1	Vertex x Interior	60	40	42	65	44	39	7.406	2.089	6.825	25.638
2	Edge x Interior	62	38	30	65	90	35	6.110	2.113	7.150	35.913
3	Vertex x Interior	100	0	30	60	3	42.5	10.922	1.998	0.000	0.225
4	Edge x Interior	98.2	1.8	50	45	90	45	9.533	2.059	7.525	54.325
5	Edge x Interior	80.4	19.6	42.6	57	50	45	9.837	2.025	6.650	23.413
6	Vertex x Interior	100	0	39.4	53.5	40	45	10.172	2.060	7.250	45.213
7	Vertex x Interior	100	0	48	45	3	42.25	10.951	2.007	0.000	1.550
8	Edge x Interior	79.7	20.3	30	45	3	35	7.298	2.072	3.575	10.688
9	Edge x Interior	80.4	19.6	30	45	90	45	9.298	2.031	6.775	24.163
10	Vertex x Interior	60	40	36	45	86	35	7.197	2.070	7.700	33.425
11	Vertex x Interior	100	0	30	45	68	42.51	9.318	2.038	8.550	42.488
12	Edge x Interior	80.3	19.7	36	65	7	35	7.877	2.067	4.363	14.325
13	Edge x Interior	99	1	30	60	68	35	7.953	2.034	8.200	34.713
14	Edge x Interior	79.3	20.7	50	65	6	42	9.281	2.023	4.863	12.831
15	Vertex x Interior	60	40	50	59.5	3	42.25	9.212	2.019	2.200	7.825
16	Edge x Interior	80.3	19.7	37	52.3	3	41.5	8.536	2.021	3.400	9.800
17	Edge x Interior	79.6	20.4	41.5	45	48	39	8.594	2.021	6.425	33.563
18	Edge x Interior	80.3	19.7	37	52.3	3	41.5	8.045	2.033	3.750	9.813
19	Vertex x Interior	100	0	48.5	59.5	3	35	8.885	2.022	0.000	1.025
20	Vertex x Interior	100	0	38	51	47	35.25	8.398	2.031	7.575	49.500
21	Vertex x Interior	60	40	42	53	43	45	9.107	2.058	6.525	25.575
22	Edge x Interior	80.4	19.6	35.4	50.3	90	35	7.263	2.050	5.600	32.638
23	Vertex x Interior	100	0	39.3	53.2	90	39	8.478	2.034	7.875	59.713
24	Edge x Interior	98	2	30	65	90	45	9.535	2.036	6.700	52.538
25	Edge x Interior	79.4	20.6	35.6	65	90	42.15	9.014	2.008	5.450	19.663
26	Vertex x Interior	60	40	37	57.8	90	41.5	8.217	2.034	6.675	31.625
27	Edge x Interior	62	38	50	65	90	45	8.994	2.036	6.450	28.500
28	Vertex x Interior	60	40	46.6	48.2	5	40.45	8.944	2.017	5.275	16.013
29	Vertex x Vertex	60	40	30	65	3	45	9.663	1.998	2.000	7.888
30	Edge x Interior	60.8	39.2	50	45	20	35	7.515	2.026	5.850	26.638
31	Edge x Interior	79.3	20.7	30	57	50	39	8.696	2.026	5.425	19.513
32	Edge x Interior	80.4	19.6	42.6	57	50	45	9.875	2.019	6.200	21.350
33	Vertex x Interior	60	40	50	58.9	86	35	7.101	2.081	7.300	34.188
34	Vertex x Interior	100	0	39.3	65	39	39.05	8.547	2.078	7.400	47.700
35	Edge x Interior	79.3	20.7	50	65	71	35	7.743	2.050	6.700	27.825
36	Edge x Interior	94.1	5.9	50	49.5	44	45	10.090	2.039	7.275	37.150
37	Edge x Interior	79.4	20.6	35.6	65	90	42.15	8.816	2.014	5.500	18.450
38	Edge x Interior	79.3	20.7	30	57	50	39	8.898	2.021	4.900	18.238
39	Vertex x Interior	60	40	35.5	59.7	3	35	7.532	2.057	2.925	10.413
40	Edge x Interior	78.7	21.3	39.1	61	57	35	7.854	2.060	6.350	23.650
41	Edge x Interior	79.8	20.2	50	45	3	45	9.476	2.008	4.450	13.450
42	Edge x Interior	79.6	20.4	50	49.9	90	42	8.694	2.018	6.450	35.200
43	Edge x Interior	99	1	50	65	3	45	11.229	1.991	0.000	0.550
44	Edge x Interior	79.6	20.4	41.5	45	48	39	8.759	2.008	6.550	30.300
45	Edge x Interior	80.6	19.4	30	65	3	45	10.807	1.981	2.325	4.863
46	Vertex x Interior	60	40	30	53	43	38.98	7.485	2.102	6.550	25.700
47	Edge x Interior	80.2	19.8	50	51	8	35	7.932	2.051	5.921	25.406
48	Edge x Interior	98	2	38.8	50.3	90	44.8	9.550	2.037	8.425	55.613
49	Vertex x Vertex	60	40	30	45	90	45	8.871	2.030	6.225	32.075
50	Vertex x Interior	100	0	33.4	45	3	35	8.904	2.015	0.000	1.375
51	Vertex x Interior	100	0	50	57.2	56	41	9.232	2.061	7.725	52.075
52	Edge x Interior	99	1	50	65	90	35	7.589	2.0534	9.800	62.013
53	Vertex x Interior	60	40	35.2	45	3	42.45	9.319	2.008	2.250	7.725
54	Vertex x Interior	60	40	50	45	85	42	8.514	2.030	6.825	30.675
55	Edge x Interior	99	1	48.5	45	66	35	8.643	1.999	7.875	41.775

The variation of WA,  $f_r$ , and  $f_c$  obtained at run (test) points is observed according to UW in Figure 3. As expected, it can be seen that WA decreases with an increase in UW. However, random variations occur in  $f_r$  and  $f_c$  depending on the change in UW. In particular, the dependence of  $f_r$  and  $f_c$  on the variation intervals of sample age (3 days - 90 days) has led to the inability to obtain significant variability between UW with  $f_r$  and  $f_c$ .

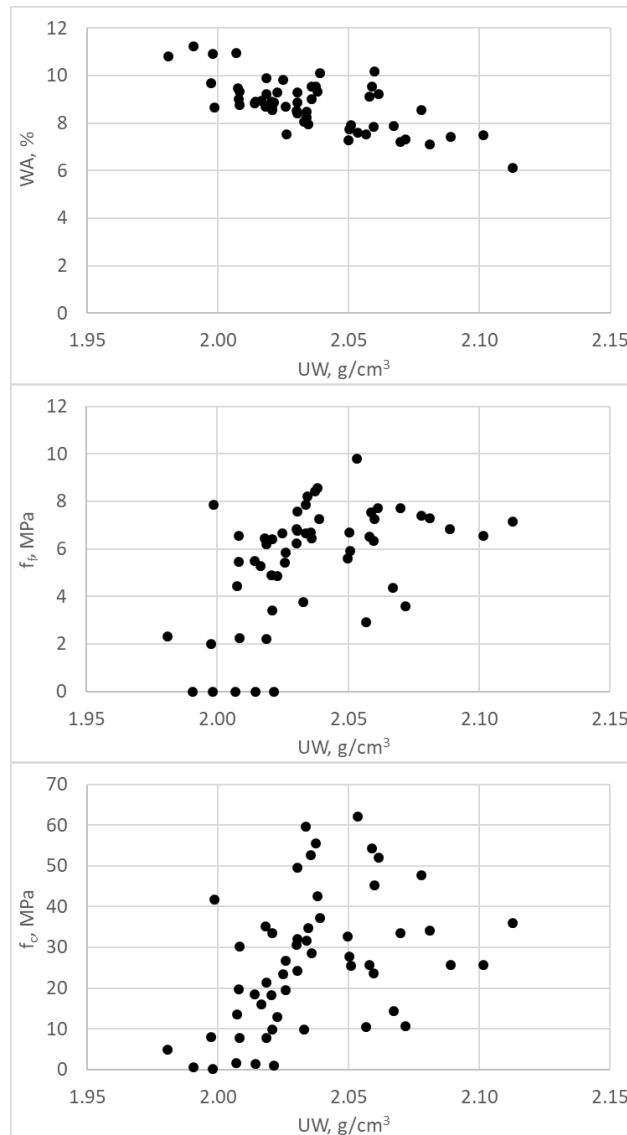


**Figure 3.** Variation of the WA,  $f_r$ , and  $f_c$  According to UW

### Statistical Analysis

The effect levels of the variables on the response variables were determined by analysis of variance. The ANOVA for WA, UW,  $f_r$ , and  $f_c$  are given in Table 5. Less than 0.0500 p-values indicate that the model terms are statistically significant (StatEase, 2021b). On the other hand, p-values higher than 0.1000 suggest that the model terms are not statistically significant (StatEase, 2021b). The models of the response variables do not include insignificant terms. Interaction and higher-order terms have significant effect levels on the response variables, as shown in Table 6. It is compatible with the complex structure of HAAC.

Lack of fit refers to the disparity observed between the actual measurements and the values anticipated by the model. When the lack of fit is statistically significant, it indicates that the divergence of the design points from their predicted values is considerably greater than the variability of the replicates around their average values. Consequently, it is preferable to have a statistically insignificant lack of fit. The significance of the lack of fit is found insignificant for the WA, UW, and  $f_c$  while significant for the  $f_r$ .

**Table 5.** ANOVA for Response Variables

Source	WA	UW	f <sub>r</sub>	f <sub>c</sub>
	p-value	p-value	p-value	p-value
<b>Model</b>	< 0.0001	< 0.0001	< 0.0001	< 0.0001
Linear Mixture	< 0.0001	< 0.0001	< 0.0001	< 0.0001
AB	0.0223	< 0.0001	0.0024	< 0.0001
AC	-	0.0314	-	< 0.0001
AD	0.0013	0.0002	-	< 0.0001
AE	< 0.0001	0.0027	< 0.0001	< 0.0001
AF	< 0.0001	0.0057	-	0.0004
BC	0.0324	0.0008	-	-
BD	0.0030	0.0004	-	-
BE	< 0.0001	< 0.0001	< 0.0001	< 0.0001
BF	< 0.0001	< 0.0001	0.0187	-
ABC	-	-	0.0005	< 0.0001
ABD	< 0.0001	0.0022	-	< 0.0001
ABE	< 0.0001	0.0005	< 0.0001	< 0.0001
ABF	-	0.0049	-	< 0.0001
ACD	-	0.0904	-	-
ACE	-	0.0229	-	0.0064
ACF	0.0771	-	-	-
ADE	0.0386	0.0063	-	< 0.0001
ADF	0.0253	0.0002	0.0123	-
AEF	0.0003	< 0.0001	-	0.0005
BCD	-	0.0059	-	0.0017
BCE	-	-	0.0450	0.0025
BCF	-	0.0003	-	-
BDE	0.0830	-	-	0.0137
BDF	0.0261	0.0048	-	-
AC <sup>2</sup>	-	0.0211	0.0172	< 0.0001
AE <sup>2</sup>	0.0026	< 0.0001	< 0.0001	< 0.0001
BC <sup>2</sup>	-	0.0810	-	-
BE <sup>2</sup>	0.0013	< 0.0001	< 0.0001	< 0.0001
ABCD	0.0023	-	-	-
ABDE	-	-	-	< 0.0001
ABEF	0.0446	-	-	-
ABC <sup>2</sup>	0.0052	-	-	0.0073
ABD <sup>2</sup>	0.0095	0.0486	-	-
ABE <sup>2</sup>	< 0.0001	< 0.0001	< 0.0001	< 0.0001
ABF <sup>2</sup>	-	0.0036	-	-
<b>Lack of fit</b>	0.4795	0.2415	0.0177	0.0683

Models in terms of L-Pseudo components and coded factors for WA, UW, f<sub>r</sub>, and f<sub>c</sub> are given in Equations 1, 2, 3, and 4. The equations, expressed in terms of coded factors, enable the prediction of responses for given levels of each factor. In this coding scheme, the high levels of the mixture components and process factors are represented as +1; the low levels of the mixture components and process factors are 0 and -1, respectively. This coded form of the equation proves valuable in assessing the relative influence of the factors by examining and comparing their respective coefficients.

$$\begin{aligned}
 \mathbf{WA} = & 9.08 \cdot A + 7.83 \cdot B + 1.12 \cdot AB - 0.2515 \cdot AD - 0.7130 \cdot AE + 0.9608 \cdot AF + 0.1308 \cdot BC - \\
 & 2126 \cdot BD - 0.4213 \cdot BE + 1.05 \cdot BF + 1.65 \cdot ABD + 1.88 \cdot ABE - 0.1270 \cdot ACF - 0.1555 \cdot ADE + \\
 & 0.1701 \cdot ADF - 0.3393 \cdot AEF - 0.1236 \cdot BDE + 0.1711 \cdot BDF + 0.3829 \cdot AE^2 + 0.4694 \cdot BE^2 - 1.04 \cdot \\
 & ABCD + 0.7367 \cdot ABEF + 1.21 \cdot ABC^2 + 1.16 \cdot ABD^2 - 4.28 \cdot ABE^2
 \end{aligned} \tag{1}$$

$$\begin{aligned}
 \mathbf{UW} = & 2.06 \cdot A + 2.08 \cdot B - 0.1801 \cdot AB + 0.0058 \cdot AC + 0.0132 \cdot AD + 0.0098 \cdot AE + 0.0086 \cdot AF - \\
 & 0.0096 \cdot BC + 0.0116 \cdot BD + 0.0126 \cdot BE - 0.0240 \cdot BF - 0.0451 \cdot ABD - 0.0515 \cdot ABE - 0.0411 \cdot \\
 & ABF + 0.0054 \cdot ACD + 0.0072 \cdot ACE + 0.0089 \cdot ADE - 0.0135 \cdot ADF + 0.0172 \cdot AEF + 0.0095 \cdot BCD + \\
 & 0.0132 \cdot BCF - 0.0096 \cdot BDF - 0.0113 \cdot AC^2 - 0.0300 \cdot AE^2 + 0.0088 \cdot BC^2 - 0.0451 \cdot BE^2 - 0.0367 \cdot \\
 & ABD^2 + 0.1785 \cdot ABE^2 + 0.0541 \cdot ABF^2
 \end{aligned} \tag{2}$$

$$\sqrt{f_f} = 2.81 \cdot A + 2.66 \cdot B - 0.9351 \cdot AB + 1.38 \cdot AE + 0.4582 \cdot BE - 0.0983 \cdot BF + 0.6693 \cdot ABC - 2.73 \cdot ABE - 0.1292 \cdot ADF - 0.0937 \cdot BCE - 0.1763 \cdot AC^2 - 1.28 \cdot AE^2 - 0.5135 \cdot BE^2 + 2.73 \cdot ABE^2 \quad (3)$$

$$\sqrt{f_c} = 7.23 \cdot A + 5.30 \cdot B - 5.24 \cdot AB + 0.3851 \cdot AC + 0.3960 \cdot AD + 3.18 \cdot AE + 0.3243 \cdot AF + 1.36 \cdot BE + 1.63 \cdot ABC - 2.49 \cdot ABD - 5.39 \cdot ABE - 2.19 \cdot ABF + 0.2544 \cdot ACE + 0.5234 \cdot ADE + 0.3404 \cdot AEF - 0.2923 \cdot BCD - 0.2636 \cdot BCE + 0.2344 \cdot BDE - 1.08 \cdot AC^2 - 2.36 \cdot AE^2 - 0.8462 \cdot BE^2 - 2.52 \cdot ABDE + 1.70 \cdot ABC^2 + 4.23 \cdot ABE^2 \quad (4)$$

The fit statistic results of the response variables are given in Table 6.  $R^2$  values for the response variables (WA, UW,  $f_f$ , and  $f_c$ ) were obtained as 0.98, 0.96, 0.98, and 0.99, respectively. The adjusted  $R^2$  value provides evidence of the substantial influence exerted by the model's adequacy and the incorporated terms on the response variable (StatEase, 2021b). Moreover, the satisfactory concurrence between the adjusted  $R^2$  and predicted  $R^2$  values (adjusted  $R^2$  - predicted  $R^2 = 0.20$  (StatEase, 2021b)) suggests that the level of variability (estimation error) present in the new data, as projected by the models, is deemed appropriate. The adjusted  $R^2$  - predicted  $R^2$  values of the models obtained for WA, UW,  $f_f$ , and  $f_c$  are 0.038, 0.130, 0.012, and 0.013, respectively.

**Table 6.** Fit Statistics of Responses

	WA	UW	$f_f$	$f_c$
<b>R<sup>2</sup></b>	0,9804	0,9552	0,9766	0,9902
<b>Adjusted R<sup>2</sup></b>	0,9648	0,9070	0,9692	0,9829
<b>Predicted R<sup>2</sup></b>	0,9271	0,7769	0,9574	0,9699

Contour plots were generated based on the effect of the independent variables on the response variables, as determined by the constructed models. Mix-process contour plots of WA, UW,  $f_f$ , and  $f_c$  are shown in Figure 4, Figure 5, Figure 6, and Figure 7, respectively.

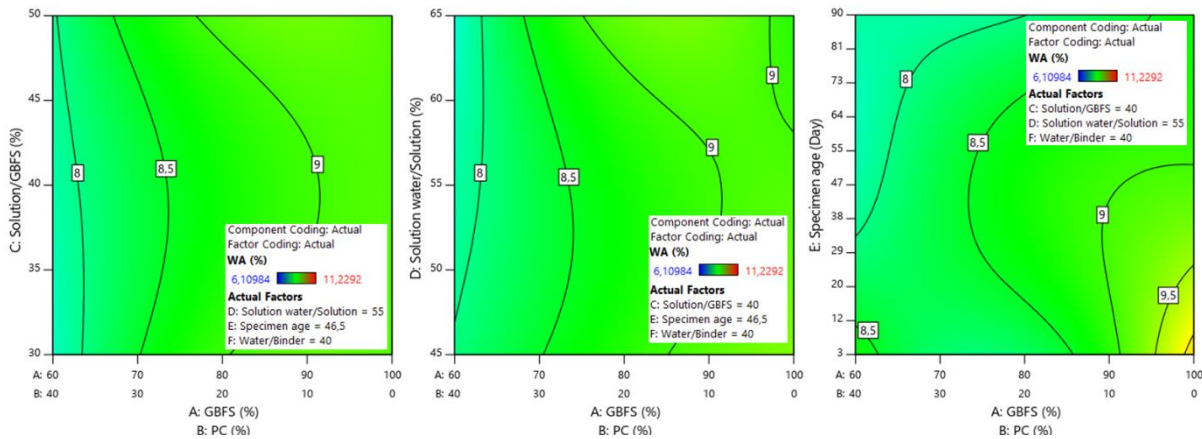


**Figure 4.** Mix-Process Contour Plots for WA

When the variation of C (Solution/GBFS ratio) is examined according to the component variable, it is observed that as PC increases in the mixture, WA decreases. This situation indicates that with the addition of PC, a more compact structure forms (Al-Kutti et al., 2018; Mohapatra & Pradhan, 2022) in the internal structure, thereby reducing the capillary voids. The variation of C does not affect WA in the range of 25%-40% of cement. However, in the range of 0-25% of cement, an increase from 30% to 40% in C does not cause variability in WA, whereas at the 40% - 50% intervals decrease in WA. The growth of a compact structure due to the increase in C-S-H gels formed by adding 25% cement and the increase in gels due to AAM resulting from the high ratio of C explains the decrease in WA.

When the variation of D (Solution water/Solution ratio) is examined according to the component variable, it is observed that WA decreases as PC increases. With the increase in D, the water content in the mixture increases. Therefore, increasing water content in the mixture is expected to increase the amount of voids. However, the internal structure gels formed with high PC addition (30%-40%) tolerate the voids that may occur as a result of the increase in water content in the mixture. However, low PC additions cannot tolerate the increasing voids.

When the change in E (Specimen age) is examined according to the component variable, it is observed that the highest WA is obtained at 0% PC ratio and 3-day specimens. This situation indicates that geopolymers do not form sufficiently due to the slow reaction rate in AAMs. As known, HAACs have higher early-age strength gain compared to AAMs (García-Lodeiro et al., 2013; Mohapatra & Pradhan, 2022). Therefore, as the PC ratio increases, WA decreases at an early age. Additionally, the compact structure formed due to the completion of both PC and AAM reactions at higher specimen ages causes WA to be low.

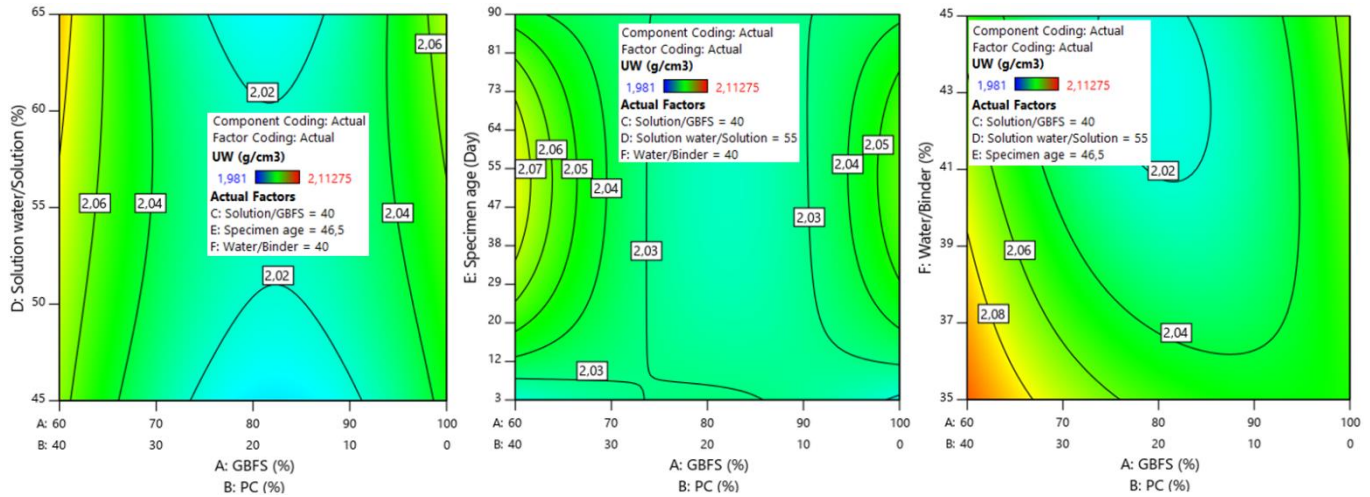


Figure 5. Mix-Process Contour Plots for UW

The variation in the solution water/solution ratio (D) does not affect UW. The compact structure in the internal structure increases with the increasing PC ratio. Therefore, UW increases with PC values above 30%. However, this increase is low (maximum UW - minimum UW = 2.08 - 2.02 = 0.06). The variation in PC creates a 0.04 g/cm<sup>3</sup> change in UW depending on the specimen age. Especially at early ages (< 7 days), it is observed that PC does not affect UW. The UW value increases as the water/binder ratio (F) decreases and PC increases. Decreasing the amount of water in the mixture reduces the number of voids, while high PC content is expected to increase UW due to the compact structure formation at high PC content.

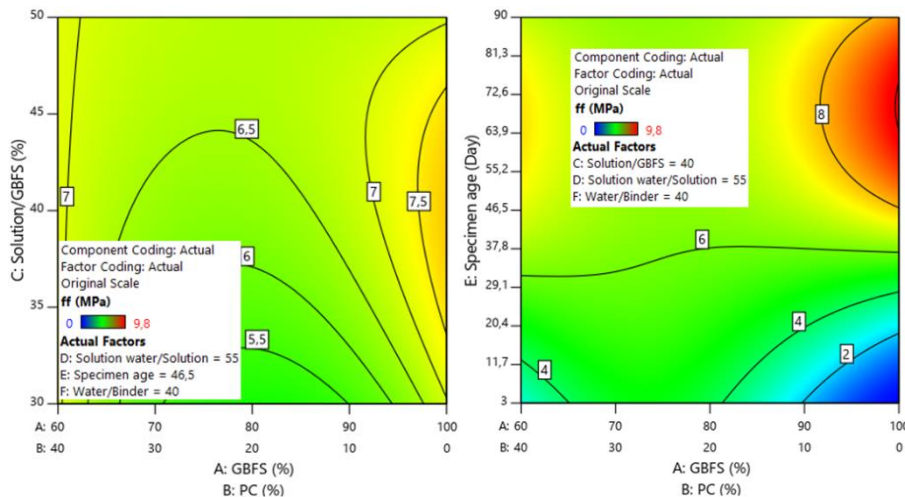


Figure 6. Mix-Process Contour Plots for  $f_f$

At low Solution/GBFS ratio (C),  $f_f$  decreases up to a PC value of 10%, while there is no change in  $f_f$  in the 10%-30% range. However,  $f_f$  increases in the 30%-40% range of PC. These variations are approximately at a level of 1 MPa (6.5 MPa - 5.5 MPa). Changes in  $f_f$  are minimal at high values of Solution/GBFS. The highest  $f_f$  value is obtained at a Solution/GBFS ratio of 40%. The highest  $f_f$  value is obtained at low PC ratios (0%-10%) and specimen ages ranging from 45 to 90 days. Moreover, an increase in the PC ratio does not affect the  $f_f$  value in 35-day specimens.

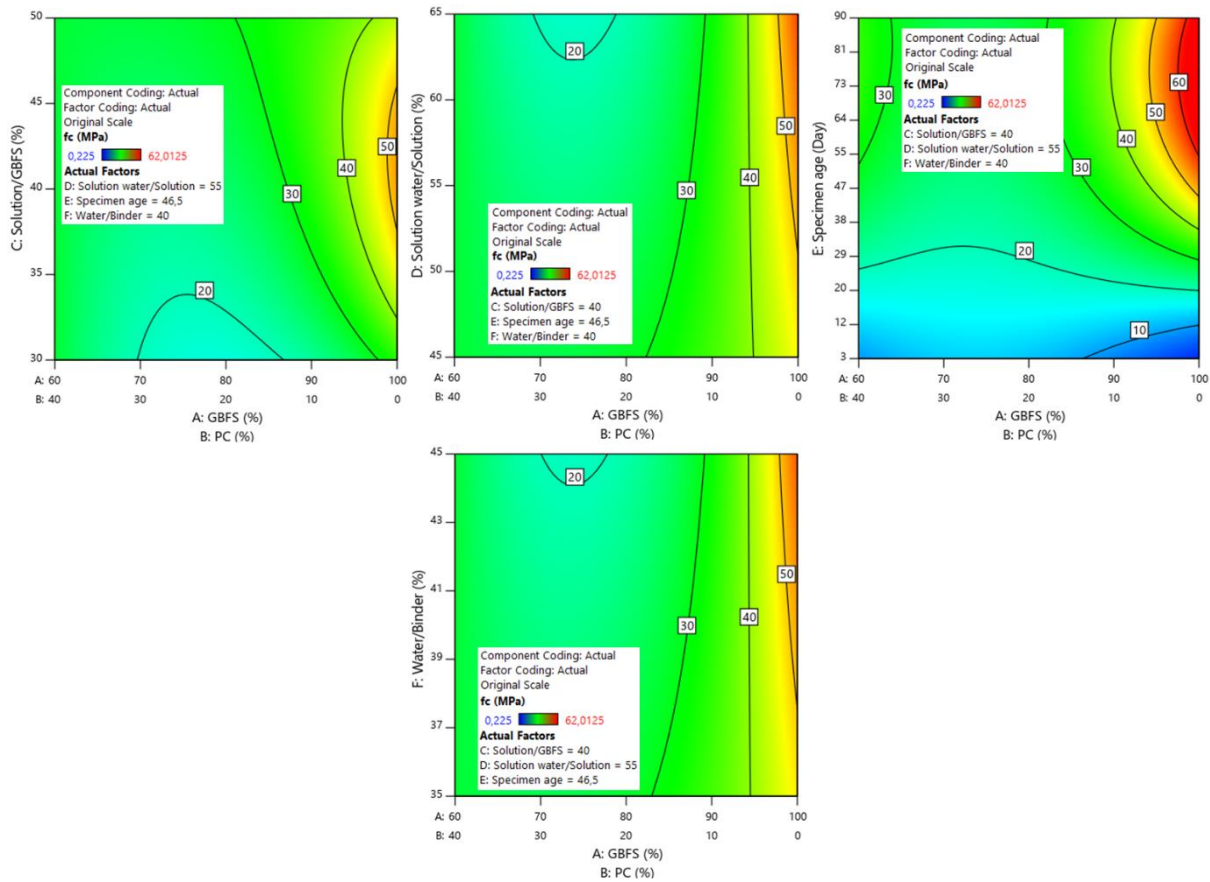


Figure 7. Mix-Process Contour Plots for  $f_c$

With an increase in Solution/GBFS (C) from 30% to 38% at 0% PC,  $f_c$  increases from 30 MPa to 50 MPa. This phenomenon can be attributed to the elevated proportion of the solution ratio, which fosters the process of alkalization. However, while  $f_c$  reaches 50 MPa in the 38%-45% range of C, there is an approximate decrease of 10 MPa in the 45%-50% range. This situation can be explained by the insufficient level of gels that should form due to alkalization in low C and an increase in the amount of water in the mixture due to the increased solution in high C, leading to an increase in the void volume. The compact structure form of the HAAC due to the high PC ratio is not sufficient to increase the  $f_c$  in low C (30%-35%). It indicates that the gels originating from AAM are not formed sufficiently in low C.

As the Solution water/Solution ratio (D) increases, in the range of 0% to 10% of PC, no variation in  $f_c$  value is observed. However, in the variation interval of 10% to 40% of PC,  $f_c$  decreases. An increase in PC leads to a decrease in GBFS, while an increase in the D increases the amount of water in the mixture or reduces the amount of solution. An increase in the mixing water increases the pore volume, or a decrease in the amount of solution at the blend reduces the reaction products of GBFS. Therefore, a decrease in  $f_c$  is an expected outcome.

An increase in specimen age (E) increases the  $f_c$ , especially when PC is 0%. For specimens with a specimen age between 55 days and 90 days and with PC at 0%, the  $f_c$  value remains unchanged and is approximately 60 MPa. An increase in PC content in specimens with low specimen ages (3 days-7 days) increases the  $f_c$  value. However, this increase is low. For specimens aged 28 days, an increase in PC does not cause a change in  $f_c$ . It has been determined that prolonged alkalization enhances  $f_c$ . Moreover, the diminution in  $f_c$  consequent to the escalation of the PC ratio for a constant E value evinces the deleterious effect of PC on alkalization. An increase in the W/B ratio (F) increase the mixing water, causing an increase in pore volume. Therefore, it is expected that an increase in the F will result in a decrease in  $f_c$ . As expected, an increase in the F entails a decrease in  $f_c$  in the range of 15% to 40% of PC. However, in the range of 0% to 15% of PC, an increase in the F does not affect  $f_c$ . Moreover, semi-protective layers can form around PC particles by the C-A-S-H gel in the HAAC systems, thereby hindering diffusion and impeding the progress of the reaction (García-Lodeiro et al., 2013; Mohapatra & Pradhan, 2022). Therefore, the presence of unreacted PC particles in the matrix due to the rising PC content at low W/B ratios also leads to a decrease in  $f_c$ .

Process contour plots of WA, UW,  $f_r$ , and  $f_c$  are shown in Figure 8, Figure 9, Figure 10, and Figure 11, respectively. When generating process contour plots, variables other than the ones of interest are kept constant at their mean values.

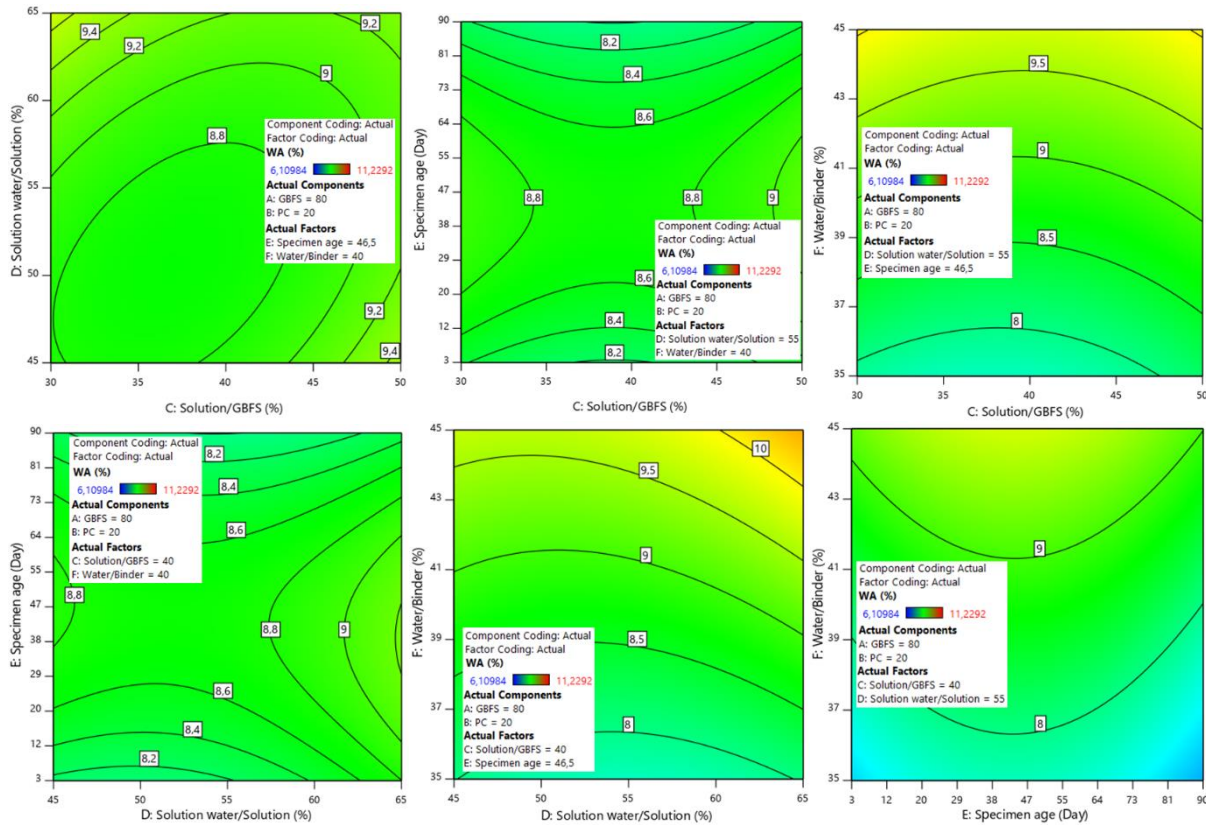


Figure 8. Process Contour Plots for WA

The response surface of WA for solution/GBFS (C) and solution water/solution (D) has been obtained as a simple minimum (Figure 8). WA is minimum at 30% - 43% and 55% - 45% variation intervals for C and D, respectively. The decrease in C and D leads to a reduction in the amount of water in the mixture, hence a decrease in WA. The response surface of WA for solution/GBFS (C) and specimen age (E) has been obtained as minimax (or saddle). Variation in C does not cause a significant change in WA. However, changes in E result in approximately a 0.6% change in WA. Due to the complex internal structure of HAACs, WA is minimally obtained at both the maximum and minimum of E. When examining the response surface of WA for solution water/solution (D) and specimen age (E), it can be said that the change in C does not create variability in WA. However, as expected, an increase in E leads to a rise in WA. The response surface of WA for solution water/solution (D) and water/binder (F) shows that the maximum WA is obtained at maximum values of D and F, where the water content in the mixture is maximum (WA, 10%). When examining the response surface of WA for specimen age (E) and water/binder (F), it is observed that the variability in WA mainly originates from F. When examining Figure 9, it can be observed that the variation range of UW is low. UW takes its lowest value due to increased mixing water, associated with maximum solution water/solution (D) and minimum solution/GBFS (C) values. An increase in specimen age (E) is expected to result in the formation of more compact structures due to the increased formation of gels in the matrix. However, it is known that in samples with high PC ratios, capillary cracks occur in the internal structure due to high hydration heat (García-Lodeiro et al., 2013). Due to the complex internal structure of specimens with 20% PC content, an increasing trend is not observed in UW only with an increase in E. The contour plot of changes in CE illustrates this situation. When examining the contour plot of CF, it can be seen that the variation in C does not significantly affect UW, but an increase in F reduces UW. An increase in F leads to a rise in the amount of water in the mixture, which increases the pore volume of the specimens and causes a decrease in UW. The contour plot of ED forms a minimax type of surface. The low values of UW are obtained at the maximum and minimum values of E and D. Maximum UW is achieved in 50%-60% and 20-75-day variation intervals for D and E, respectively. When examining the contour plot of DF, minimum UW is obtained at maximum F and D. As the maximum values of F and D result in maximum water content in the mixture, leading to a high amount of pores in the specimen, UW is low. UW value is minimum at the minimum E and the maximum F values. Moreover, the level of variation in UW due to changes in F is higher than the effect of specimen age.

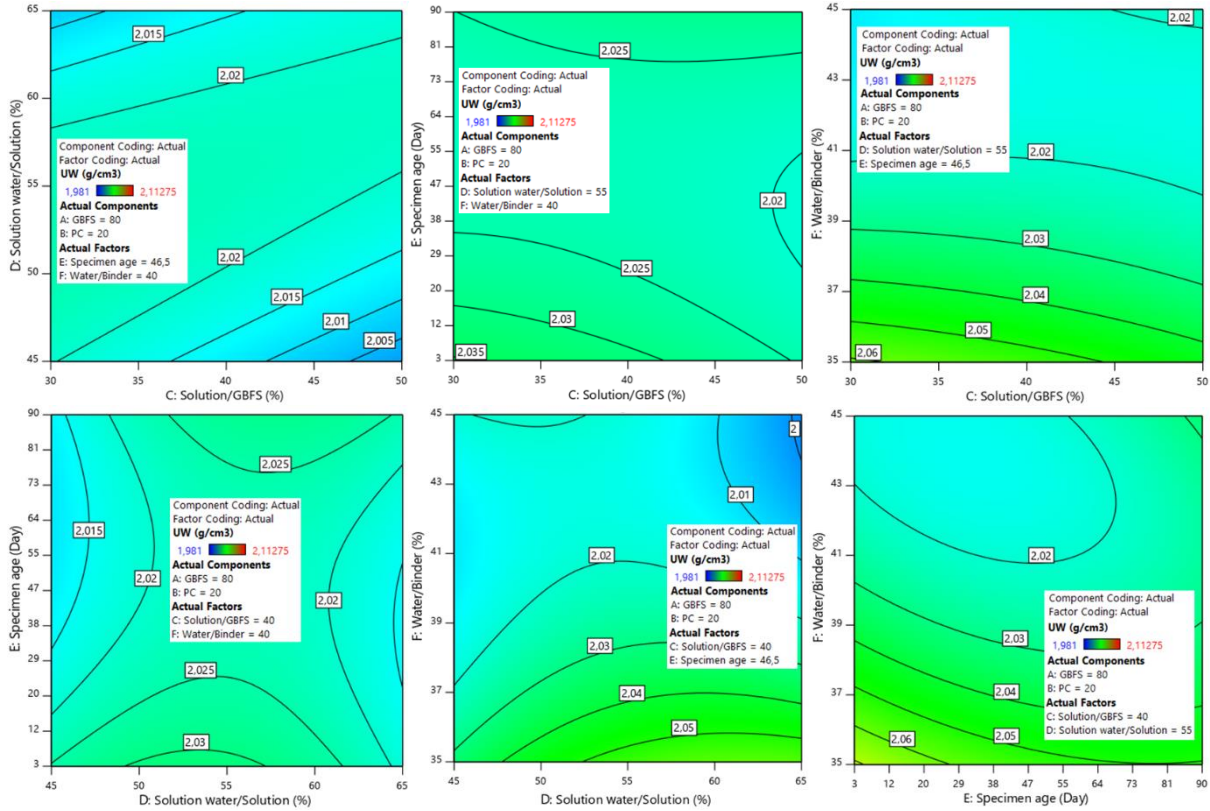


Figure 9. Process Contour Plots for UW

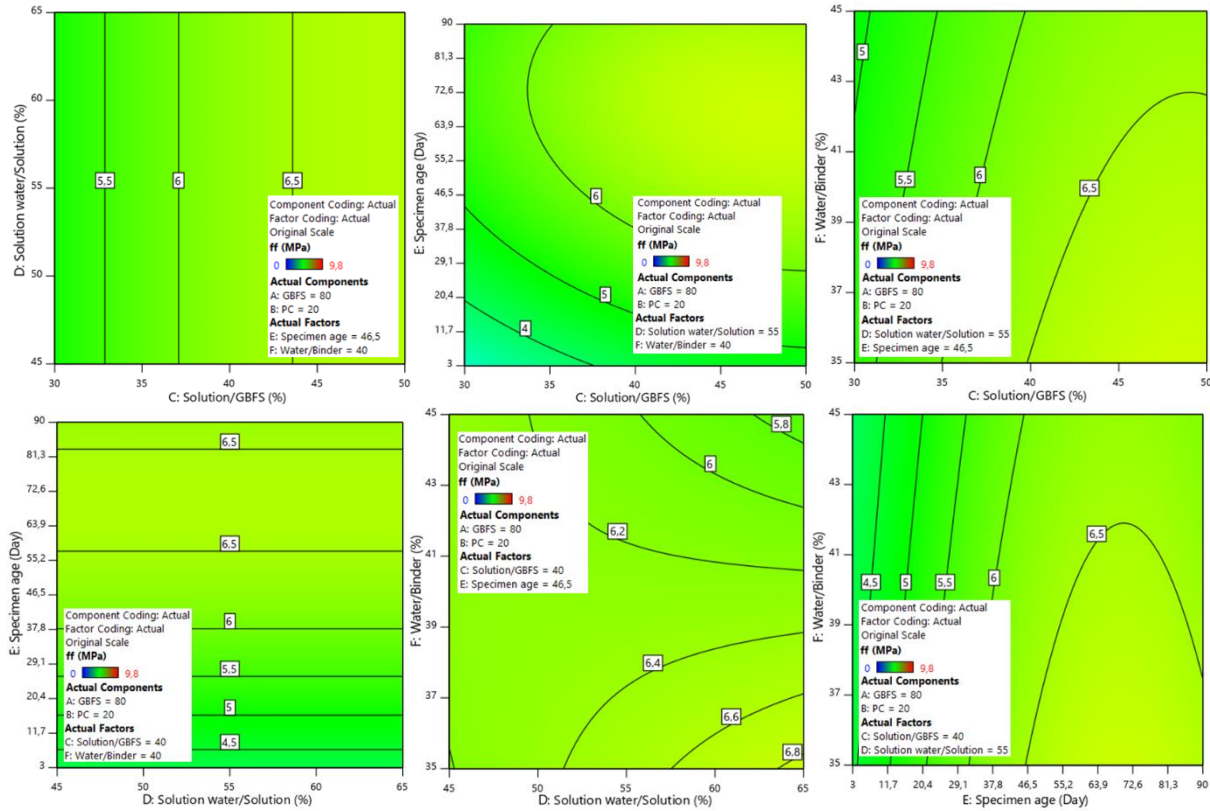


Figure 10. Process Contour Plots for  $f_f$

In the contour plot of CD, it can be observed that the variation in D does not affect  $f_f$ . An increase in the amount of solution in the mixture leads to a rise in the alkalinization of GBFS particles, consequently increasing  $f_f$ . In the  $f_f$  contour plot dependent on CE, it is seen that  $f_f$  is maximum at the maximum values of C and E. High  $f_f$  values (6 MPa) are obtained even at high values of C, especially at low specimen ages. Response surface for CF, it is observed

that maximum  $f_f$  is obtained at minimum F and maximum C. Additionally, high values of C, resulting in high water content in the mixture, i.e., an increase in F, do not significantly affect  $f_f$ . According to the DE contour plot, a change in E increases the  $f_f$  value, while a change in D does not affect the  $f_f$  value. In the DF contour plot,  $f_f$  is minimum at maximum D and minimum F. The maximum value of  $f_f$  is obtained at maximum D and minimum F. The EF contour plot shows that an increase in F in the 3-45-day-old specimens does not cause a change in  $f_f$ . However, increasing F from 42% to 45% in the 45-90-day specimens leads to a decrease in  $f_f$ .

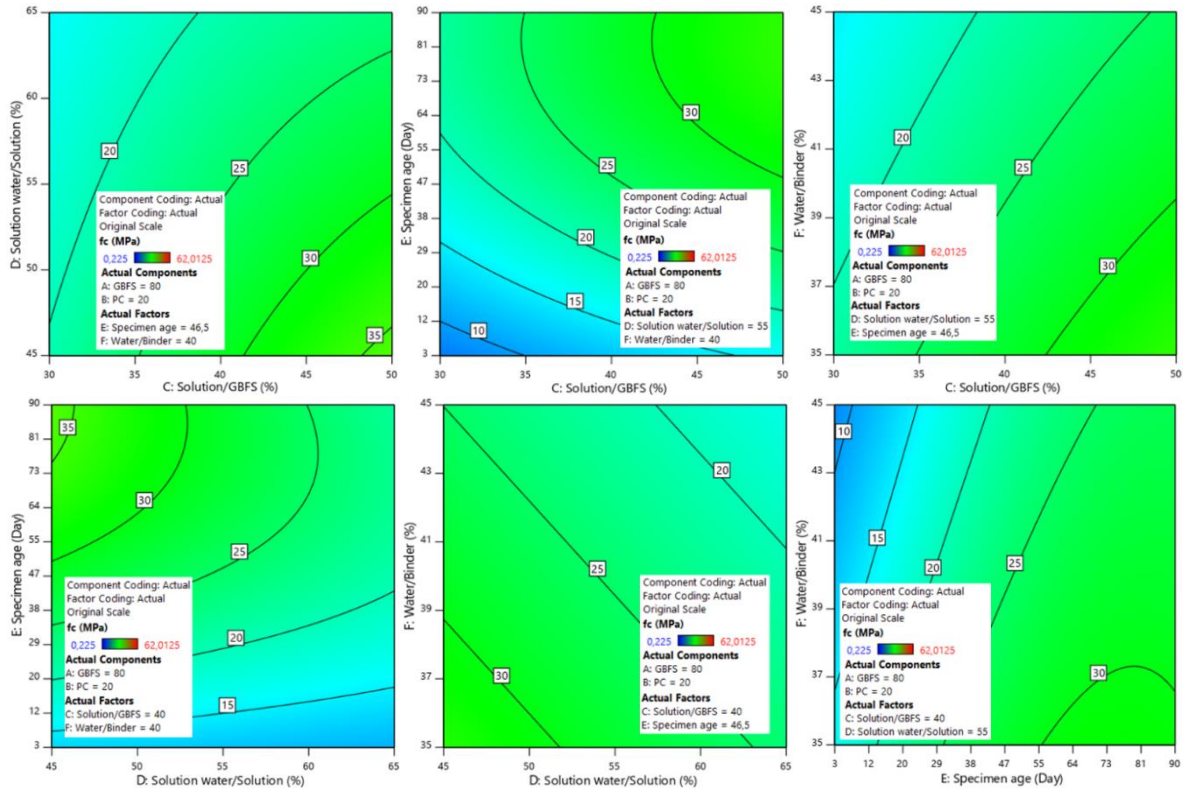


Figure 11. Process Contour Plots for  $f_c$

When examining the process contour plots for  $f_c$ , it can be seen that maximum  $f_c$  is obtained at the maximum values of E and C and minimum values of F and D. As known, the amounts of gels formed due to hydration and alkalinization increase depending on the specimen age (E). As F decreases, the amount of water in the mixture decreases, leading to a decrease in pore volume and an increase in  $f_c$ . The actual and predicted values for the response variables are shown in Figure 12 and Figure 13. The actual and the predicted values of the response variables (WA, UW,  $f_f$  and  $f_c$ ) exhibit a significant overlap ( $R^2 > 0.95$ ) for the selected variations intervals of effect variables. The absolute maximum residuals (actual minus predicted) for the WA, UW,  $f_f$  and  $f_c$  are 0.3798, 0.0163, 0.4859 and 0.4115, respectively. According to the results obtained for the response variables, the highest standard deviation is observed in  $f_c$ . It indicates that the variability in  $f_c$  is higher compared to other response variables. Therefore, although the absolute maximum residual for  $f_c$  (0.4115) is higher than that for WA (0.3798) and UW (0.0163), the linearity deviation of the actual and predicted values is lower.

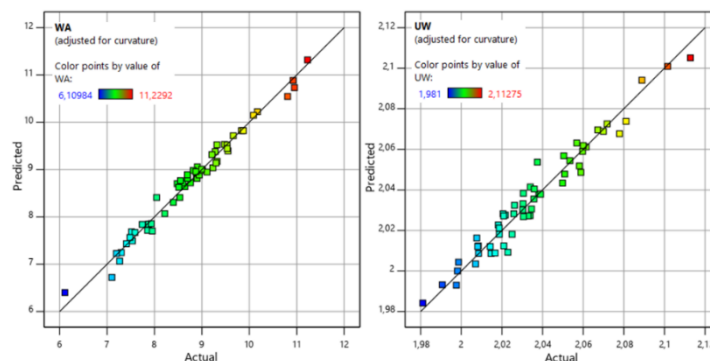


Figure 12. Predicted and Actual Values for WA and UW

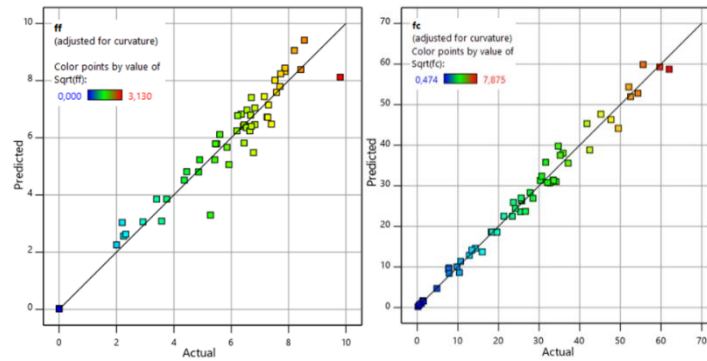


Figure 13. Predicted and Actual Values for  $f_f$  and  $f_c$

**Multi-Variable Optimization**

The optimum values of the response variables are determined using the desirability function. Three different goals have been set for optimization. The first goal considers only the mechanical properties, the second goal considers only the physical properties, and the third goal takes into account both the physical and mechanical properties' optimum values. The optimization of the response variables is given in Table 7. Upon examining the solution results obtained based on the goals, it is observed that the desired goals can be achieved at high specimen ages. This is mainly due to the wide variation intervals in specimen age. Because the time required for the formation of gels in the internal structure, which primarily affects the mechanical properties, is high in HAAC materials. Therefore, suitable and applicable curing conditions need to be determined for the improvement of early-age strength in AAMs and HAACs. It is observed that the addition of PC to the mixture does not lead to improvement in mechanical properties (Solution<sup>1</sup>; PC: %0), but it does result in improvement in physical properties (Solution<sup>2</sup>; PC: %40). The desirability for optimizing both mechanical and physical properties in HAACs is 0.9130. Therefore, in the use of HAACs, it is necessary to determine the necessary optimum conditions depending on environmental conditions and design accordingly.

Table 7. Optimization of Response Variables

Name	A:GBFS	B:PC	C:Solution /GBFS	D:Solution water/ Solution	E:Specimen age	F:Water /Binder	WA	UW	$f_f^{**}$	$f_c^{**}$	Combined desirability
Goal <sup>1</sup>	is in range	is in range	is in range	is in range	is in range	is in range	none	none	Max.	Max.	
Goal <sup>2</sup>	is in range	is in range	is in range	is in range	is in range	is in range	Min.	Max.	none	none	
Goal <sup>3</sup>	is in range	is in range	is in range	is in range	is in range	is in range	Min.	Max.	Max.	Max.	
Lower Limit	60	0	30	45	3	35	6.1098	1.981	0	0.4743	
Upper Limit	100	40	50	65	90	45	11.229	2.1128	3.1305	7.8748	
Lower Weight	1	1	1	1	1	1	1	1	1	1	
Upper Weight	1	1	1	1	1	1	1	1	1	1	
Imp.*	3	3	3	3	3	3	3	3	3	5	
Solution <sup>1</sup>	100	0	46.1	60	74	37	8.151	2.058	3.141	68.310	
Solution <sup>2</sup>	60	40	30.0	65	72	35	6.110	2.136	2.905	40.751	
Solution <sup>3</sup>	60	40	30.0	65	82	35	6.134	2.125	2.869	42.709	
Desirability <sup>1</sup>	1	1	1	1	1	1	-	-	1	1	
Desirability <sup>2</sup>	1	1	1	1	1	1	1	1	-	-	1
Desirability <sup>3</sup>	1	1	1	1	1	1	0.9953	1	0.9165	0.8190	0.9130

<sup>1</sup>Optimization for mechanical properties, <sup>2</sup>Optimization for physical properties, <sup>3</sup>Optimization for mechanical+physical properties

\*Importance, \*\*Lower and upper limit values were given in transformation applied form.

**CONCLUSIONS**

In this study, multi-variable optimization of physical and mechanical properties of hybrid alkali-activated blast furnace slag mortars was investigated. The results obtained in the study are given below (GBFS ratio: A, PC ratio: B, solution/GBFS: C, solution water/solution: D, specimen age: E, water/binder: F, water absorption: WA, unit weight: UW, flexural strength:  $f_f$ , compressive strength:  $f_c$ ).

- The flow-table values of mortar specimens change from 10.1 to 20.4 cm. HAAC specimens' workability decreases with an increase in the PC ratio.
- The HAAC specimens' maximum  $f_c$  value was obtained from the 52nd run point (A: 99%, B: 1%, C: 50%, D: 65, E: 90, F: 35%, WA: 7.6, UW: 2.05,  $f_r$ : 9.8,  $f_c$ : 62). When the 52nd trial point is examined, it is seen that the effect variable values that maximize  $f_c$  are the expected values.
- The relationship between WA and UW is inversible. However,  $f_r$  and  $f_c$  exhibit random variations depending on the change in UW because the variation intervals of the sample age (3 days - 90 days) are large, and the reactions of GBFS and cement are quite slow in the early days.
- The response variable models exclude insignificant terms. Interaction and higher-order terms significantly affect the response variables, which is consistent with the complex structure of HAAC.
- The lack of fit is not significant for WA, UW, and  $f_c$  while it is significant for  $f_r$ .
- The adjusted  $R^2$  - predicted  $R^2$  values of the models obtained for WA, UW,  $f_r$ , and  $f_c$  are less than 0.2 and are 0.038, 0.130, 0.012, and 0.013, respectively. This indicates that the variability level (prediction error) present in the new data predicted by the models is appropriate.
- The process contour plots for  $f_c$  indicate that the highest E, C, and the lowest F and D, result in the maximum  $f_c$ . It is well-established that the amount of gels formed due to hydration and alkalization increases with specimen age (E). Therefore, as F decreases, the water content in the mixture also decreases, leading to a reduction in pore volume and an increase in  $f_c$ .
- The actual and predicted values of response variables (WA, UW,  $f_r$ , and  $f_c$ ) exhibit a significant overlap ( $R^2 > 0.95$ ) within the selected variation intervals of effect variables.
- The standard deviation for  $f_c$  is the highest. The variability in  $f_c$  is higher than that of other response variables. Despite  $f_c$  having a higher absolute maximum residual (0.4115) compared to WA (0.3798) and UW (0.0163), its linearity deviation of actual and predicted values is lower.
- The desired goals are more likely to be achieved at high specimen ages because specimen age intervals are wide range. Because the gel formation in the internal structure of HAACs requires time, it significantly affects the mechanical properties. Determining the suitable and applicable curing conditions is crucial for improving early-age strength in AAMs and HAACs.
- PC addition to the mixture does not improve mechanical properties, but it improves physical properties. The desirability for optimizing mechanical (100% PC), physical (60% PC), and mechanical/physical (60% PC) properties in HAACs is 1, 1, and 0.913, respectively. Therefore, it is crucial to determine the optimum conditions based on environmental factors and design accordingly.

Future research to investigate the effect of controllable factors such as activator combinations, different pozzolans, and curing methods on the mechanical and physical properties of HAAC will contribute significantly to the advancement of HAAC technology. Furthermore, permeability, sulfate/corrosion resistance, and electrical/thermal conductivity will provide valuable insights into achieving the optimum properties of HAAC. In addition, Artificial Intelligence (AI) techniques to determine the optimum mechanical and physical properties based on the effect variables of HAACs would be highly beneficial.

## STATEMENTS AND DECLARATIONS

### *Acknowledgement*

This research did not receive any specific grant from funding agencies in the public, commercial, or not-for-profit sectors.

### *Competing Interest*

The authors have no competing interests to declare that are relevant to the content of this article.

### *Author Contributions*

Conceptualization: [Yunus Emre Avşar; Mehmet Timur Cihan; İbrahim Feda Aral], Data Curation: [Yunus Emre Avşar; Mehmet Timur Cihan; İbrahim Feda Aral], Formal analysis: [Mehmet Timur Cihan], Investigation: [Yunus Emre Avşar; Mehmet Timur Cihan], Methodology: [Yunus Emre Avşar; Mehmet Timur Cihan; İbrahim Feda Aral], Project administration: [Yunus Emre Avşar], Resources: [Yunus Emre Avşar; Mehmet Timur Cihan], Supervision: [Mehmet Timur Cihan], Validation: [Yunus Emre Avşar; Mehmet Timur Cihan], Visualization: [Yunus Emre Avşar; Mehmet Timur Cihan], Roles/Writing - Original Draft [Yunus Emre Avşar; Mehmet Timur Cihan], Writing - Review & Editing: [Yunus Emre Avşar; Mehmet Timur Cihan; İbrahim Feda Aral].

### **Artificial Intelligence Contribution Statement**

This manuscript was entirely written, edited, analyzed, and prepared without the assistance of any artificial intelligence tools. All content, including text, data analysis, and figures, was solely generated by the authors.

### **REFERENCES**

- Aliabdo, A.A., Abd Elmoaty, A.E.M., & Emam, M.A. (2019). Factors affecting the mechanical properties of alkali activated ground granulated blast furnace slag concrete. *Construction and Building Materials*, 197, 339-355. <https://doi.org/10.1016/j.conbuildmat.2018.11.086>
- Al-Kutti, W., Nasir, M., Megat Johari, M.A., Islam, A.B.M.S., Manda, A.A., & Blaisi, N.I. (2018). An overview and experimental study on hybrid binders containing date palm ash, fly ash, OPC and activator composites. *Construction and Building Materials*, 159, 567-577. <https://doi.org/10.1016/j.conbuildmat.2017.11.017>
- Amer, I., Kohail, M., El-Feky, M.S., Rashad, A., & Khalaf, M.A. (2021). Characterization of alkali-activated hybrid slag/cement concrete. *Ain Shams Engineering Journal*, 12(1), 135-144. <https://doi.org/10.1016/j.asej.2020.08.003>
- Amer, I., Kohail, M., El-Feky, M.S., Rashad, A., & Khalaf, M.A. (2020). Evaluation of using cement in alkali-activated slag concrete. *International Journal of Scientific and Technology Research*, 9, 245-248
- Ameri, F., Shoaie, P., Reza Musaei, H., Alireza Zareei, S., & Cheah, C.B. (2020). Partial replacement of copper slag with treated crumb rubber aggregates in alkali-activated slag mortar. *Construction and Building Materials*, 256, 119468. <https://doi.org/10.1016/j.conbuildmat.2020.119468>
- Angulo-Ramírez, D.E., Mejía de Gutiérrez, R., & Puertas, F. (2017). Alkali-activated Portland blast-furnace slag cement: Mechanical properties and hydration. *Construction and Building Materials*, 140, 119-128. <https://doi.org/10.1016/j.conbuildmat.2017.02.092>
- Askarian, M., Tao, Z., Adam, G., & Samali, B. (2018). Mechanical properties of ambient cured one-part hybrid OPC-geopolymer concrete. *Construction and Building Materials*, 186, 330-337. <https://doi.org/10.1016/j.conbuildmat.2018.07.160>
- Avşar, Y.E., & Cihan, M.T. (2023). Multi-response optimization of mechanical properties of alkali-activated mortars. *Arabian Journal for Science and Engineering*, 48, 13871-13887. <https://doi.org/10.1007/s13369-023-07957-9>
- Bilim, C., & Atiş, C.D. (2012). Alkali activation of mortars containing different replacement levels of ground granulated blast furnace slag. *Construction and Building Materials*, 28(1), 708-712. <https://doi.org/10.1016/j.conbuildmat.2011.10.018>
- Box, G.E., & Cox, D.R. (1964). An analysis of transformations. *Journal of the Royal Statistical Society: Series B (Methodological)*, 26(2), 211-243. <https://doi.org/10.1111/j.2517-6161.1964.tb00553.x>
- Chokkalingam, P., El-Hassan, H., El-Dieb, A., & El-Mir, A. (2022). Multi-response optimization of ceramic waste geopolymer concrete using BWM and TOPSIS based taguchi methods. *Journal of Materials Research and Technology*, 21, 4824-4845. <https://doi.org/10.1016/j.jmrt.2022.11.089>
- Derringer, G., & Suich, R. (2018). Simultaneous optimization of several response variables. *Journal of Quality Technology*, 12(4), 214-219. <https://doi.org/10.1080/00224065.1980.11980968>
- Escalante, J.I., Gómez, L.Y., Johal, K.K., Mendoza, G., Mancha, H., & Méndez, J. (2001). Reactivity of blast-furnace slag in Portland cement blends hydrated under different conditions. *Cement and Concrete Research*, 31(10), 1403-1409. [https://doi.org/10.1016/S0008-8846\(01\)00587-7](https://doi.org/10.1016/S0008-8846(01)00587-7)
- Fang, G., Ho, W.K., Tu, W., & Zhang, M. (2018). Workability and mechanical properties of alkali-activated fly ash-slag concrete cured at ambient temperature. *Construction and Building Materials*, 172, 476-487. <https://doi.org/10.1016/j.conbuildmat.2018.04.008>
- Francis Yakobu, K., Ravichandran, P.T., Sudha, C., & Kannan Rajkumar, P.R. (2015). Influence of GGBS on rheology of cement paste and concrete with SNF and PCE based superplasticizers. *Indian Journal of Science and Technology*, 8(36), 1-7. <https://doi.org/10.17485/ijst/2015/v8i36/87539>
- García-Lodeiro, I., Fernández-Jiménez, A., & Palomo, A. (2013). Variation in hybrid cements over time. Alkaline activation of fly ash-portland cement blends. *Cement and Concrete Research*, 52, 112-122. <https://doi.org/10.1016/j.cemconres.2013.03.022>

- García-Lodeiro, I., Maltseva, O., Palomo, A., & Fernández-Jiménez, A. (2012). Hybrid alkaline cements Part I: Fundamentals. *Revista Romana de Materiale/Romanian Journal of Materials*, 42, 330-335
- Jindal, B.B. (2019). Investigations on the properties of geopolymer mortar and concrete with mineral admixtures: A review. *Construction and Building Materials*, 227, 116644. <https://doi.org/10.1016/j.conbuildmat.2019.08.025>
- Khan, S.U., Nuruddin, M.F., Ayub, T., & Shafiq, N. (2014). Effects of different mineral admixtures on the properties of fresh concrete. *The Scientific World Journal*, 4, 986567. <https://doi.org/10.1155/2014/986567>
- Law, D.W., Adam, A.A., Molyneaux, T.K., & Patnaikuni, I. (2012). Durability assessment of alkali activated slag (AAS) concrete. *Materials and Structures/Materiaux et Constructions*, 45, 1425-1437. <https://doi.org/10.1617/s11527-012-9842-1>
- Mohapatra, A.K., & Pradhan, B. (2022). Hybrid alkali activated cements (HAACs) system: A state of the art review on fresh, mechanical, and durability behaviour. *Construction and Building Materials*, 361, 129636. <https://doi.org/10.1016/j.conbuildmat.2022.129636>
- Myers, R.H., Montgomery, D.C., & Anderson-Cook, C.M. (2009). Response surface methodology: Process and product optimization using designed experiments. New Jersey: Wiley
- Nath, P., & Sarker, P.K. (2014). Effect of GGBFS on setting, workability and early strength properties of fly ash geopolymer concrete cured in ambient condition. *Construction and Building Materials*, 66, 163-171. <https://doi.org/10.1016/j.conbuildmat.2014.05.080>
- Patel, Y.J., & Shah, N. (2018). Enhancement of the properties of ground granulated blast furnace slag based self compacting geopolymer concrete by incorporating rice husk ash. *Construction and Building Materials*, 171, 654-662. <https://doi.org/10.1016/j.conbuildmat.2018.03.166>
- Provis, J.L., Duxson, P., & Van Deventer, J.S.J. (2010). The role of particle technology in developing sustainable construction materials. *Advanced Powder Technology*, 21(1), 2-7. <https://doi.org/10.1016/j.apt.2009.10.006>
- Saha, S., & Rajasekaran, C. (2017). Enhancement of the properties of fly ash based geopolymer paste by incorporating ground granulated blast furnace slag. *Construction and Building Materials*, 146, 615-620. <https://doi.org/10.1016/j.conbuildmat.2017.04.139>
- Schneider, M., Romer, M., Tschudin, M., & Bolio, H. (2011). Sustainable cement production-present and future. *Cement and Concrete Research*, 41(7), 642-650. <https://doi.org/10.1016/j.cemconres.2011.03.019>
- Scrivener, K.L., & Nonat, A. (2011). Hydration of cementitious materials, present and future. *Cement and Concrete Research*, 41(7), 651-665. <https://doi.org/10.1016/j.cemconres.2011.03.026>
- Shi, X., Zhang, C., Wang, X., Zhang, T., & Wang, Q. (2022). Response surface methodology for multi-objective optimization of fly ash-GGBS based geopolymer mortar. *Construction and Building Materials*, 315, 125644. <https://doi.org/10.1016/j.conbuildmat.2021.125644>
- Shoaei, P., Ameri, F., Reza Musaei, H., Ghasemi, T., & Cheah, C.B. (2020). Glass powder as a partial precursor in Portland cement and alkali-activated slag mortar: A comprehensive comparative study. *Construction and Building Materials*, 251, 118991. <https://doi.org/10.1016/j.conbuildmat.2020.118991>
- StatEase. Design-Expert (Version 11.0.5.0 64-bit). (2021b). [www.statease.com](http://www.statease.com)
- StatEase. Desirability function. (2021a). <https://www.statease.com/docs/v11/contents/optimization/desirability-function/> Accessed 23.11.23
- Suwan, T., & Fan, M. (2014). Influence of OPC replacement and manufacturing procedures on the properties of self-cured geopolymer. *Construction and Building Materials*, 73, 551-561. <https://doi.org/10.1016/j.conbuildmat.2014.09.065>
- Topçu, İ.B. (2013). High-volume ground granulated blast furnace slag (GGBFS) concrete. *Eco-Efficient Concrete*, 218-240. <https://doi.org/10.1533/9780857098993.2.218>
- TSE. (2000). TS EN 1015-3 Methods of test for mortar for masonry-Part 3: Determination of consistence of fresh mortar (by flow table). Ankara: Turkish Standards Institution
- TSE. (2016). TS EN 196-1 Methods of testing cement-Part 1: Determination of strength. Ankara: Turkish Standards Institution

Xue, L., Zhang, Z., & Wang, H. (2021). Early hydration kinetics and microstructure development of hybrid alkali activated cements (HAACs) at room temperature. *Cement and Concrete Composites*, 123, 104200. <https://doi.org/10.1016/j.cemconcomp.2021.104200>

Yang, K.H., Song, J.K., Ashour, A.F., & Lee, E.T. (2008). Properties of cementless mortars activated by sodium silicate. *Construction and Building Materials*, 22(9), 1981-1989. <https://doi.org/10.1016/j.conbuildmat.2007.07.003>